Bioorganic & Medicinal Chemistry 17 (2009) 1514–1526

Contents lists available at ScienceDirect

Bioorganic & Medicinal Chemistry

journal homepage: www.elsevier.com/locate/bmc

The flexibility of the Le^aLe^x Tumor Associated Antigen central fragment studied by systematic and stochastic searches as well as dynamic simulations

Trudy A. Jackson [a], Valerie Robertson [a], Anne Imberty [b], France-Isabelle Auzanneau [a,*]

[a] Department of Chemistry, University of Guelph, Guelph, Ontario, Canada N1G 2W1
[b] CERMAV-CNRS (Affiliated with Université Joseph Fourier and Member of the Institut de Chimie Moléculaire de Grenoble), BP 53, F-38041, Grenoble Cedex 9, France

ARTICLE INFO

Article history:
Received 15 October 2008
Revised 2 January 2009
Accepted 8 January 2009
Available online 15 January 2009

Keywords:
Carbohydrate-based anti-cancer vaccines
Le^aLe^x
Conformational analysis
NMR spectroscopy
Stochastic search
Systematic search
Molecular dynamics
Synthesis

ABSTRACT

The solution conformational behavior of the Tumor-Associated Carbohydrate Antigen Le^aLe^x central fragment: methyl α-L-fucopyranosyl-(1→4)-2-acetamido-2-deoxy-β-D-glucopyranosyl-(1→3)-β-D-galactopyranoside was studied using three computational methods: a rigid systematic search as implemented in Sybyl, a stochastic search as implemented in MOE2004, and dynamics simulations using the SANDER module of AMBER9. Our results illustrate the complementarity of these methods to identify energetically relevant conformations and flexible linkages. In particular, the β-GlcNAc-(1→3)-Gal linkage was shown to be extremely flexible adopting a wide range of orientations around two energy minima. The modeling results were validated by comparison of theoretical distances, derived from the simulations, with experimental measurements obtained from 1D selective ROESY buildup curves on the synthetic fragment.

1. Introduction

Tumor-Associated Carbohydrate Antigens (TACAs) are interesting targets for the development of anti-cancer vaccines. One such TACA, the Le^aLe^x hexasaccharide **1**, has been shown to be over-expressed at the surface of squamous lung carcinoma cells.[1–3] However, to date, this hexasaccharide has not been extensively investigated for efficacy in anti-cancer vaccines because its terminal non-reducing Le^a trisaccharide is also commonly expressed on normal non-tumor cells.[4] Thus, polyclonal antibodies generated from a vaccine based on the hexasaccharide will likely cross-react with Le^a leading to autoimmune reactions. However, a monoclonal antibody 43-9F that was raised against Le^aLe^x, has shown high selectivity toward internal epitopes of the hexasaccharide, while it did not bind efficiently to the terminal trisaccharide residue.[5–7] With the ultimate goal to develop a selective anti-tumor vaccine, we have embarked on the identification of such internal Tumor-Associated Carbohydrate Epitopes (TACE) and have undertaken detailed studies of internal fragments of the hexasaccharide **1**. Here we describe an improved synthesis of the central Le^aLe^x trisaccharide fragment: methyl α-L-fucopyranosyl-(1→4)-2-acetamido-2-deoxy-β-D-glucopyranosyl-(1→3)-β-D-galactopyranoside **2** than that previously reported.[8] The conformational properties of the trisaccharide were investigated by both rigid systematic and relaxed stochastic molecular mechanics searches and by molecular dynamics simulations in explicit solvent. The modeling results were validated by comparison of theoretical distances derived from the simulations with experimental measurements obtained from ROESY spectra at several mixing times.

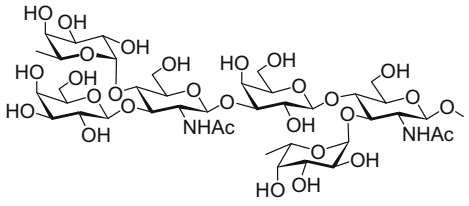

1

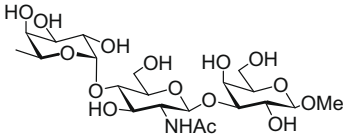

2

* Corresponding author. Tel.: +1 519 824 4120; fax: +1 519 766 1499.
E-mail addresses: Anne.Imberty@cermav.cnrs.fr (A. Imberty), fauzanne@uouelph.ca (F.-I. Auzanneau).

0968-0896/$ - see front matter © 2009 Elsevier Ltd. All rights reserved.
doi:10.1016/j.bmc.2009.01.020

2. Results and discussion

2.1. Synthesis of trisaccharide 2

For the synthesis of the trisaccharide fragment, we envisaged a '1 + 1 + 1' linear addition of the monosaccharide precursors. We first attempted the regioselective glycosylation of the known[9] diol **4** (Scheme 1) with the known[10] donor **3**. The reaction was carried out in CH_2Cl_2 at −78 °C, using an excess of acceptor **4** (1.5 equiv) and under promotion by TMSOTf (0.16 equiv). However under these conditions, neither the desired 3-O-glycosylated disaccharide nor its regioisomer glycosylated at O-4 were observed and the only product isolated in 76% yield was the di-O-glycosylated trisaccharide **5**. Thus, in contrast to previous reports of such selective glycosylation at O-3 of galactosyl residues in lactoside acceptors,[11] there was no significant difference in reactivities between O-3 and O-4 in the monosaccharide diol acceptor **4** that would allow its selective glycosylation. Abandoning this regioselective strategy, we prepared acceptor **6** selectively free at O-3 in 81% yield by treating diol **4** with trimethyl orthobenzoate under acid catalysis and opening the resulting orthoester by treatment with aq AcOH (Scheme 2).

This constitutes an alternative synthesis of tribenzoate **6**, which had previously been obtained[12] via the palladium catalyzed debenzylation of methyl 2,4,6-tri-*O*-benzoyl-3-*O*-benzyl-β-D-galactopyranoside. Coupling of the alcohol **6** with the donor **3** starting at −78 °C, adding up to 0.5 equiv of TMSOTf, and allowing the reaction to reach room temperature over 18 h resulted only in the silylation of the acceptor. In contrast, carrying out the glycosylation at −30 °C with up to 2.0 equiv of TMSOTf and continuous stirring overnight at −30 °C successfully afforded the desired disaccharide **7** in 88% yield. Disaccharide **7** was subsequently converted to the acceptor **11** in four synthetic steps (Scheme 2). Selective deacetylation (2% HCl in MeOH) gave the triol **8** in 77% yield and that was converted to the benzylidene acetal **9** [$PhCH(OMe)_2$/TsOH]. Acetylation of the crude alcohol **9** gave disaccharide **10** (94%) which was reductively opened yielding the desired acceptor **11** (86%). The regioselectivity of the benzylidene ring opening was confirmed by acetylation of an analytical sample of acceptor **11** yielding acetate **12**. Indeed, ^1H NMR showed that signal H-4′ appeared at 4.84–4.95 ppm in compound **12**, while this signal was found upfield at 3.66 ppm in acceptor **11**, supporting that O-4′ was indeed acetylated in **12** and free in acceptor **11**. The disaccharide acceptor **11** was then glycosylated with the known[13] β- or α-fucose thioethyl donors **13** or **14** under promotion with MeOTf to yield trisaccharide **15** in 85% and 77% yield, respectively (Scheme 3). The trisaccharide **15** was deprotected in three steps (72% overall

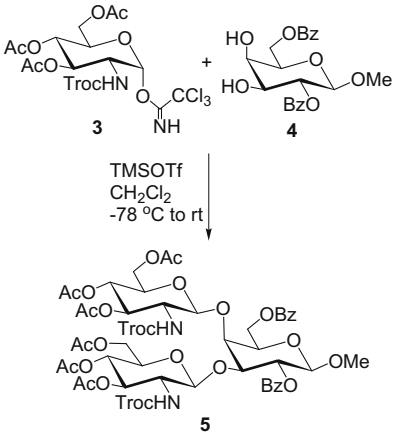

Scheme 1.

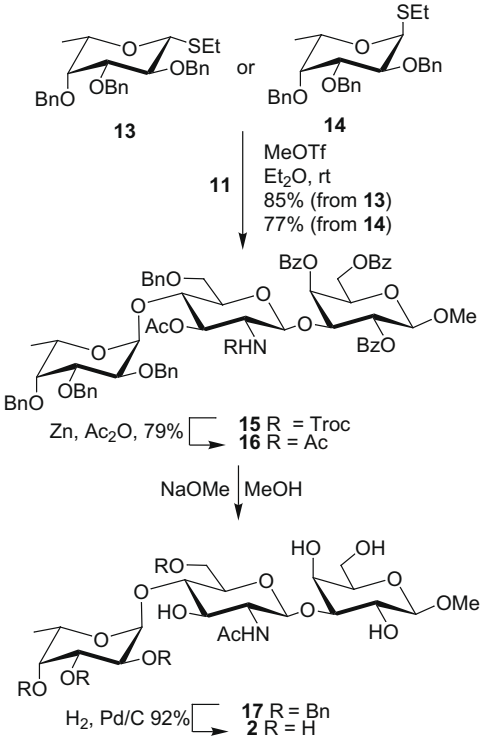

Scheme 3.

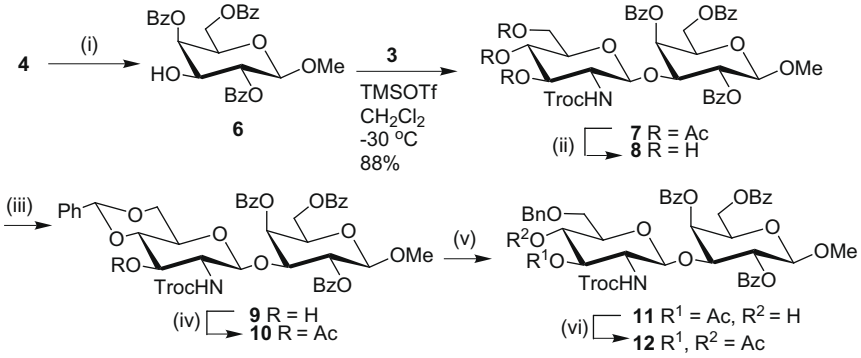

Scheme 2. Reagents and conditions: (i) (a) $PhC(OMe)_3$, TsOH, DMF; (b) 80% AcOH; 81%. (ii) HCl/MeOH, 77%. (iii) $PhCH(OMe)_2$, TsOH, DMF. (iv) Ac_2O, C_6H_5N, 94%. (v) $NaCNBH_3$, HCl–Et_2O, THF, 86%. (vi) Ac_2O, C_6H_5N, 68%.

yield): treatment with Zn dust in acetic anhydride gave the *N*-acetate **16** which was submitted to Zemplén deacylation followed by catalytic hydrogenation. From the protected monosaccharides, the overall yield of our synthesis was 34% a considerable improvement over the previously reported synthesis of **2** in which the trisaccharide was obtained in 11% yield from protected monosaccharides.[8] Having this fragment of Le^aLe^x in hand we proceeded to study its conformational behavior using a combination of NMR experiments and computational methods.

2.2. NMR measurements

The ^1H and ^{13}C chemical shift assignments and $^3J_{H,H}$ coupling constants for trisaccharide **2** were determined by a combination of 1D and 2D NMR experiments. The ^{13}C chemical shift values are in close agreement with values reported previously.[8] The vicinal coupling constants measured for the three sugar units supported an average $^4C_1$ conformation for the galactose and *N*-acetylglucosamine rings and a $^1C_4$ conformation of the fucose ring. Interresidue NOE interactions were evaluated using 2D NOESY experiments at 300 and 310 K as well as 1D selective ROESY experiments at 300 K. At 300 K, the molecular tumbling rate of trisaccharide **2** was such that at 600 MHz NOESY signals were not of sufficient intensity for quantification even when increasing the number of scans eight fold or increasing sample concentration. Dilution of the NMR sample and increasing of the temperature to 310 K to reduce sample viscosity and decrease τ_c allowed the collection of usable NOE data. Figure 1 shows the significant region of the NOESY spectrum obtained in these conditions at 800 ms mixing time. The molecular tumbling rate of the trisaccharide was sufficiently fast such that $\omega\tau_c$ was less than 1.12, and cross-peaks in the NOESY spectra were positive when the diagonal was phased as negative. All expected intra-residue cross-peaks were evident: medium to strong cross-peaks were observed for the glycosidic protons H-1″/H-4′ and H-1′/H-3, weak to medium cross-peaks were observed for H-1″/H-6′a and H-1″/H-6′b as well as H-1′/H-4 (Fig. 1). However, the %NOEs were still low (~1.2%), and the signal-to-noise ratio at this temperature required that the buildup curves be fitted only to points at high mixing times (400 ms–1 s, see Supplementary data). Thus, we acquired 1D ROESY experiments at 300 K, selectively irradiating H-1′ and H-1″. As can be seen in Figure 2, these experiments gave significantly better signal intensities and cross relaxation buildup curves could be obtained over mixing times ranging from 20 ms to 400 ms. Distances were evaluated using the initial slopes of the normalized cross relaxation buildup curves (Fig. 3) fitted to a double exponential equation. The R^2 values for these fits were at least 0.999 in every instance. These results are compared below to the outcome of our computational studies of the conformational behavior of trisaccharide **2**.

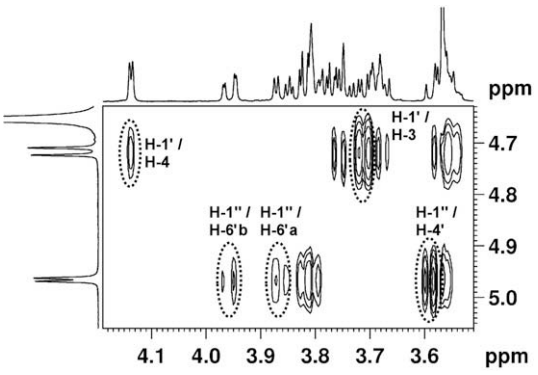

Figure 1. 600 MHz NOESY spectrum recorded at 310 K (800 ms mixing time).

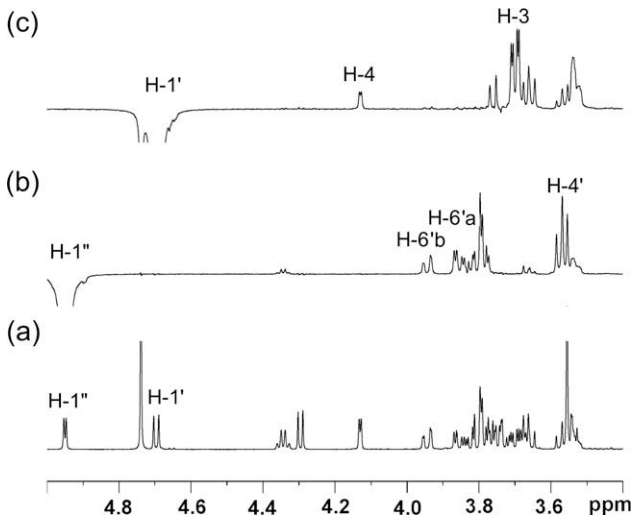

Figure 2. (a) ^1H NMR spectrum (600 MHz, 300 K) of trisaccharide **2**; (b) ^1H, ^1H ROESY spectrum (mixing time 100 ms) upon selective excitation of proton H-1″; (c) ^1H, ^1H ROESY spectrum (mixing time 100 ms) upon selective excitation of proton H-1′.

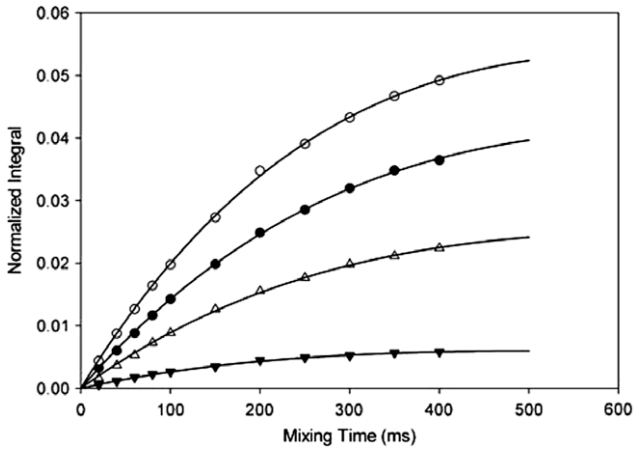

Figure 3. ^1H, ^1H ROESY cross-relaxation build up curves for proton pairs H-1′/H-3 (○), H-1′/H-4 (▼), H-1′/H-3′ (Δ), H-1″/H-4′ (●).

2.3. Computational studies

The different orientations around the glycosidic linkages of oligosaccharides have the most substantial impact on the overall molecular shape,[14] and are therefore often the main underlying determinant of binding properties to receptors such as antibodies.[15] We therefore focused our attention on the conformational features associated with these linkages in the trisaccharide. The orientations adopted around the glycosidic linkages are described by two dihedral angles: Φ = O5–C1–O1–Cx and Ψ = C1–O1–Cx–Cx + 1. The signs of the torsions are in agreement with the recommendations of the IUPAC-IUB Commission of Biochemical Nomenclature.[16]

2.3.1. Rigid search: potential energy surface of trisaccharide 2

Rigid-residue searches provide computationally efficient means of studying potential energy surfaces and identifying key minima of molecules.[14] Rigid isoenergy contour maps were calculated for trisaccharide **2** using the Tripos[17] force field with the inclusion of the PIM[18] parameters for carbohydrates. For each trisaccharide linkage the resulting Φ–Ψ map has been superimposed over the

previously reported relaxed energy maps of the corresponding constituent disaccharide (Fig. 4a and b).[19] As can be seen in Figure 4a and b, the overall conformational space as well as the locations of minima agree closely with those obtained for the disaccharides. For the β-GlcNAc-(1→3)-Gal linkage (Fig. 4a), the low-energy areas identified for the rigid search (colored surfaces) are almost identical to those obtained for the disaccharide MM3 grid search[19] (black contours).

The potential energy surface displays four principal minima **A**–**D**. The global minimum **A**, as well as local minima **B** and **C** adopt linkage conformations corresponding to the preferred exo-anomeric Φ^1 orientations[20] while the local minimum **D** adopts a syn Φ^1 orientations. For the Ψ^1 linkage, minima **A** and **D** correspond to (+) gauche orientation whereas minimum **B** fits an anti orientation and **C** a (−) gauche orientation. This potential energy map (Fig. 4a) suggests that the conformationally accessible region surrounding the **D** minimum is more extended for the trisaccharide than for the corresponding disaccharide.

In contrast to the β-GlcNAc-(1→3)-Gal linkage (Fig. 4a), the diameters of the energy plateaus surrounding the minima for the α-Fuc-(1→4)-GlcNAc linkage of the trisaccharide (colored surface Fig. 4b) are marginally more restricted than for the MM3 grid searches of corresponding disaccharide[19] (black contours Fig. 4b). However, it is difficult to say whether this indicates any reduced flexibility of this linkage in the trisaccharide relative to the disaccharide since this discrepancy can also be explained by the various approximations inherent to the rigid-residue approach.[14] For this linkage, the potential energy map shows two main minima **A′** and **B′** (Fig. 4b). The Φ^2 torsions of these minima both correspond to the preferred orientation directed by the exo-anomeric effect.[20] Minimum **A′**, which is the global minimum for the disaccharide, corresponds to a (−) gauche orientation of the Ψ^2 linkage, whereas minimum **B′** corresponds to a (+) gauche orientation. Overall, the fewer minima found for the α-Fuc-(1→4)-GlcNAc linkage suggests less potential flexibility for this linkage than for the β-GlcNAc-(1→3)-Gal linkage.

2.3.2. Stochastic search: conformational families of trisaccharide 2

Mapping the potential energy surface of the trisaccharide, and identifying the main accessible low-energy plateaus, provides a good starting point for predicting its solution conformational behavior. However, it is possible that subtle structural variations around the main minima significantly impact the overall shape

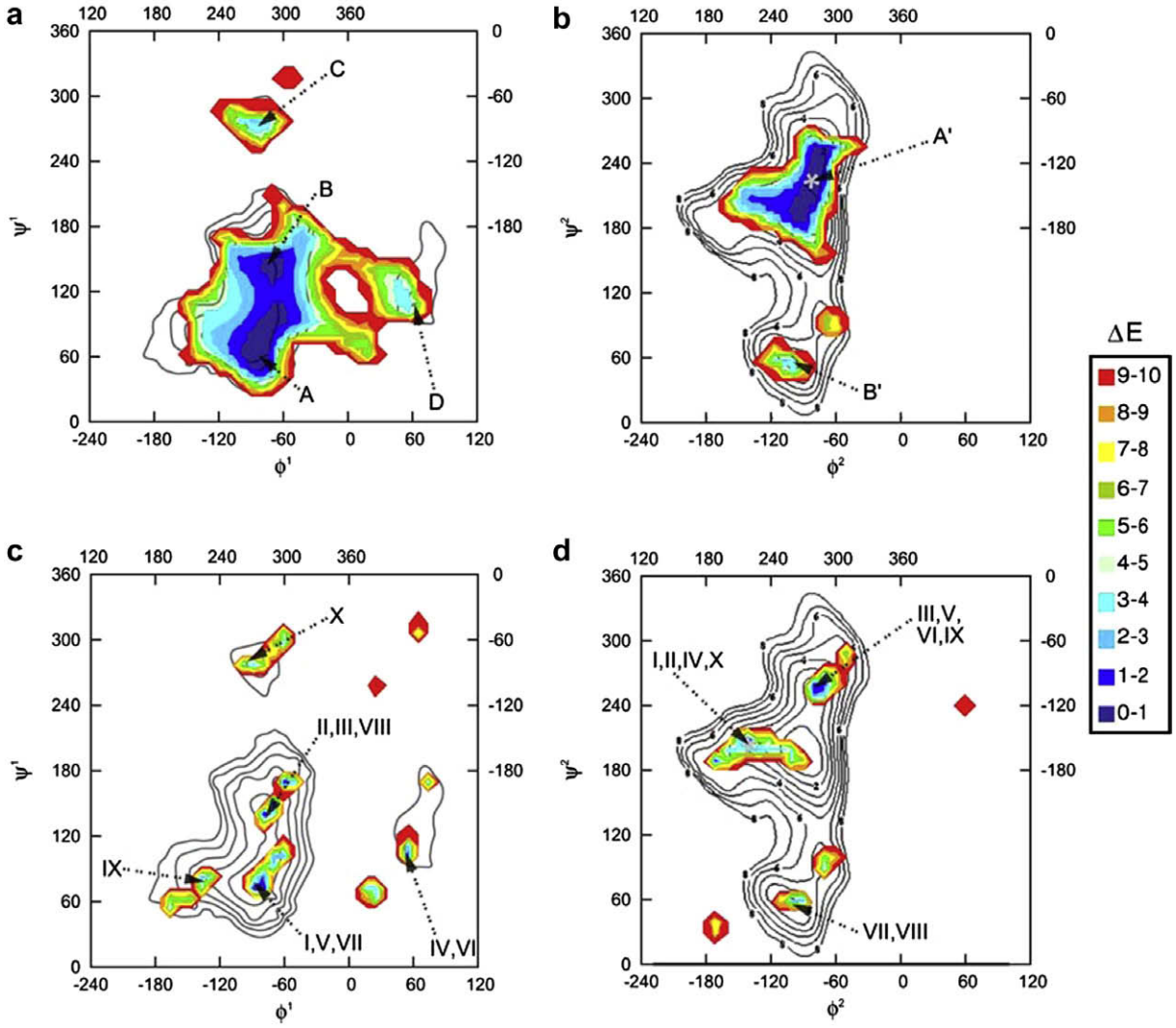

Figure 4. Potential energy maps of the glycosidic linkages of trisaccharide **2** superimposed on the energy maps obtained from previous MM3 grid searches for the corresponding disaccharide linkages (black contours).[19] (a) β-GlcNAc-(1→3)-Gal linkage and (b) α-Fuc-(1→4)-GlcNAc linkage: PIM rigid systematic search (colored); (c) β-GlcNAc-(1→3)-Gal linkage and (d) α-Fuc-(1→4)-GlcNAc linkage: MOE stochastic search (colored).

of the molecule. In addition, the energetically accessible combinations of torsions around the glycosidic linkages are not readily apparent from the energy maps of each linkage considered in isolation. Thus, we proceeded to attempt the identification of such combination via stochastic searches using the AMBER94 force field[21] as it is implemented in the Molecular Operating Environment (MOE2004) software package.[22] In these stochastic searches, minima in the potential energy surface are randomly sampled through the rotation of all bonds (including ring bonds) to random dihedral angles as well as through a random 0.4 Å Cartesian perturbation of atom positions. Two searches of 150,000 iterations were carried out to generate new conformers that were each minimized with implicit solvation by the Generalized Born/Surface Area (GB/SA) continuum solvation model.[23] In the first search an RMS tolerance of 0.01 Å on heavy atoms was used to determine whether generated conformations were considered as new. In the second search an RMS tolerance of 0.1 Å was applied on all atoms including all hydrogen atoms to account for possible hydrogen bonding. The databases were combined and only those conformations found within 10 kcal/mol from the global minimum were retained, resulting in 1450 conformers. The potential energy maps obtained for the two glycosidic linkages are shown as colored surfaces in Figure 4c and d superimposed over the maps of the constituent disaccharides shown as black contours. The minima located for the individual linkages are in good agreement with the low-energy areas previously identified for the corresponding disaccharides as well as those obtained for the trisaccharide from the Tripos PIM rigid systematic search. However, as can been seen when comparing Figure 4a and c for the β-GlcNAc-(1→3)-Gal linkage as well as Figure 4b and d for the α-Fuc-(1→4)-GlcNAc linkage, the low energy areas identified in the stochastic search appear to be much more restricted than in those found by the PIM rigid search. This results from the fact that such stochastic searches are unlikely sampling the entire conformational space. In fact, our searches did not meet the 'number of failures to find new conformations' termination criteria (10,000 iterations in a row), and terminated at the end on the 150,000 iterations. The conformations obtained within 3 kcal/mol of the global minimum were clustered into families based upon orientations around the two sets of Φ and Ψ linkages. A conformation was considered as belonging to a different family if at least one of its glycosidic torsions differed by more than 30° from another conformation. Ten different conformational families (**I**–**X**) were identified and the lowest energy representative conformations of each family are identified in Figure 4c and d.

For the β-GlcNAc-(1→3)-Gal linkage, 7 out of the 10 families adopt orientations that belong to the same energy plateau as minima **A** and **B** identified in the systematic searches, of which 3 families correspond to minimum **A** and 3 to minimum **B**. Two families were found to belong to the plateau in which the rigid search orientation **D** was found and one conformational family was identified in the energy plateau that contained orientation **C** found by the rigid search. For the α-Fuc-(1→4)-GlcNAc linkage, the energy plateau that includes the minimum orientation **A**′ identified by the systematic search dominates the trisaccharide families, and conformations close to this minimum are adopted in 8 of the 10 families identified. The plateau represented by the orientation **B**′ found in the systematic search is identified in the remaining two families.

When comparing the global minimum found by the stochastic search (I, Fig. 4c and d) to that found by the rigid search (**AA**′, Fig. 4a and b), we noticed that the Φ^2 torsions of the α-Fuc-(1→4)-GlcNAc linkage differed by 70° (compare Fig. 4b and d) while the remaining torsions were found to be in excellent agreement with one another. This difference is likely resulting from the different parameterizations of the force fields involved. Indeed, for both the MOE AMBER94 and TRIPOS PIM global minima, further optimization using AM1 semi-empirical calculations with implicit COSMO solvation led to an identical conformation with an intermediate Φ^2 torsion of −110°. Thus, the orientations obtained from the two force fields are both likely to be close in energy and closely associated with the true global minimum orientation. Globally, three conformational families (**I**, **V**, **IX**) were found to present orientations for the two glycosidic bonds belonging to the energy plateaus surrounding a combined **AA**′ global minimum identified by the systematic search. Similarly, two conformational families (**II**, **III**) corresponded to orientations close to a combined **BA**′ local minimum and two families (**IV**, **VI**) were found that corresponded to a **DA**′ combined local minimum. The remaining families of higher energy (**VII**, **VIII**, **X**) corresponded, respectively to combined local minima **AB**′, **BB**′ and **CA**′. Overall, the stochastic search and the rigid search gave conformational profiles that were in good agreement and the stochastic search complemented well the rigid search by showing three combinations of glycosidic torsions that seem to be energetically favored: the global minimum **AA**′ and two local minima **BA**′ and **DA**′ (Fig. 4). As shown below these early conclusions were in full agreement with the molecular dynamics simulations and NMR experiments.

2.3.3. Molecular dynamics simulations: flexibility of trisaccharide 2

Molecular dynamics simulations at 300 and 310 K were carried out using AMBER9[24] with the inclusion of Glycam04 parameters for carbohydrates.[25] We ran trajectories of 8 ns in explicit water starting from the global minimum (**AA**′) obtained in the Tripos-PIM systematic search. The average values of the Φ and Ψ dihedral angles for both glycosidic linkages as well as the associated calculated standard deviations are given in Table 1, entries 1 and 2.

The superimposition of the Φ–Ψ trajectories for each linkage over the adiabatic maps for the corresponding disaccharides[19] are shown in Figure 5 and the variations of the individual glycosidic torsions for the length of the simulation are shown in Figure 6.

The data obtained when running the dynamic simulation at 300 K and seen in Figures 5a, b and 6a, b show that at this temperature both the β-GlcNAc-(1→3)-Gal and α-Fuc-(1→4)-GlcNAc linkages remained in the same energy plateau. With respect to the β-GlcNAc-(1→3)-Gal linkage, the trisaccharide remained in the low-energy region surrounding the global minimum **A**, and local minimum **B** throughout most of the simulation. Standard deviations values of 22° and 24°, for the Φ^1 and Ψ^1 torsions, respectively (Table 1, entry 1) showed that there were significant fluctuations around these torsions such that the entire low-energy region was explored and the multiple distinct conformational families associated with the minima **A** and **B** energy wells were visited.

Table 1
Calculated torsion angles[a]

Entry		Φ^1	Ψ^1	Φ^2	Ψ^2
Molecular dynamics simulations[b]					
	T (K)				
1	300	−90	94	−85	−130
		±22[c]	±24[c]	±16[c]	±24[c]
2	310	−74	101	−94	−132
		±52[c]	±30[c]	±26[c]	±23[c]
Rigid search conformations[d]					
3	**AA**′	−79	58	−76	−147
4	**BA**′	−73	148	−76	−146
5	**DA**′	62	104	−76	−142

[a] Φ^1, Ψ^1 = β-GlcNAc-(1→3)-Gal; Φ^2, Ψ^2 = α-Fuc-(1→4)-GlcNAc.
[b] Average torsions calculated for the MD simulations.
[c] Standard deviation.
[d] Selected from the rigid search and minimized with the Tripos-PIM force field.

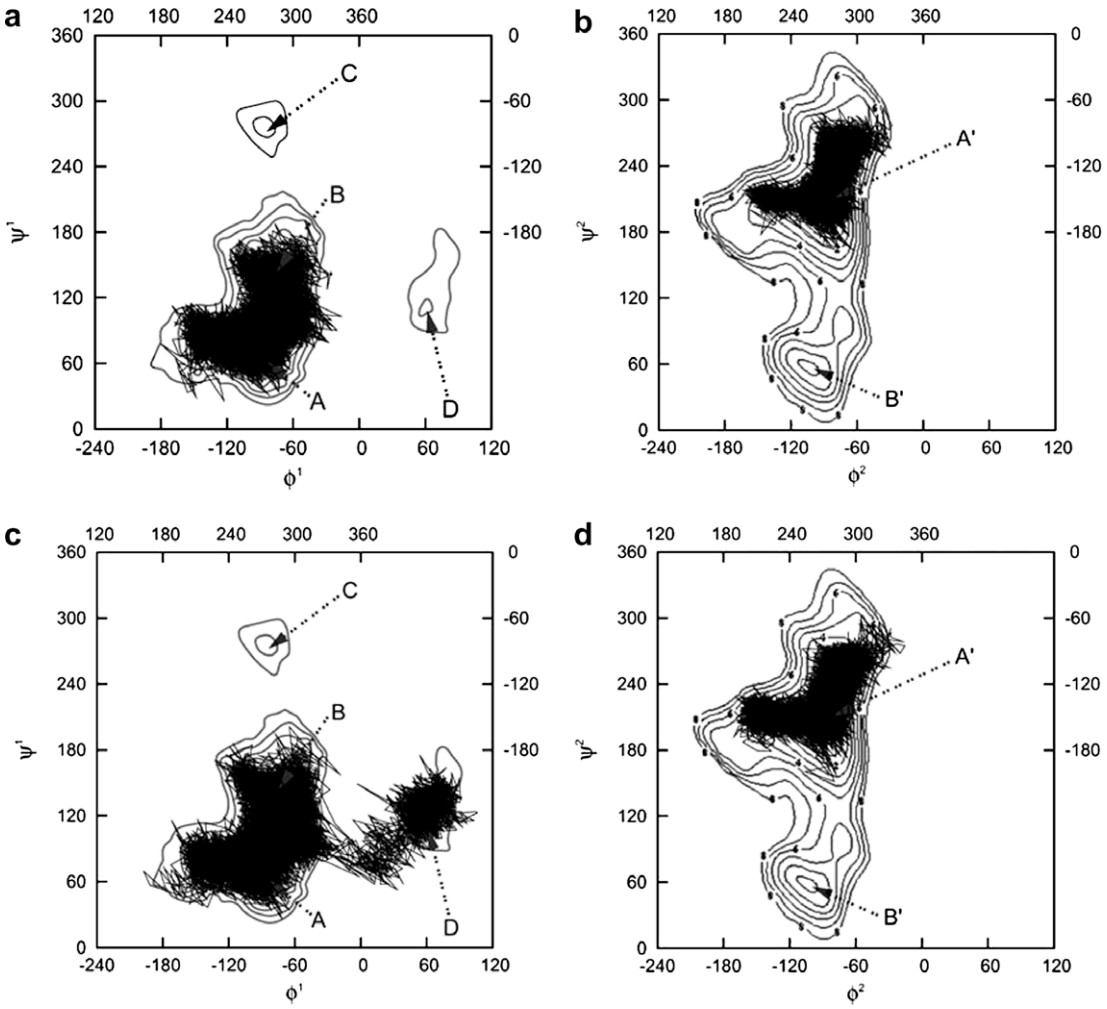

Figure 5. Trajectories of the glycosidic torsion angles Φ, Ψ during the 8 ns dynamics simulations at 300 K (a and b) and 310 K (c and d) superimposed on the MM3 grid search energy maps obtained for the disaccharide linkages (contours).[19] The main minima identified in the PIM rigid systematic search are labeled A–D and A′, B′. (a) and (c) Φ^1, Ψ^1 for the β-GlcNAc-(1→3)-Gal linkage; (b) and (d) Φ^2, Ψ^2 for the α-Fuc-(1→4)-GlcNAc linkage.

The α-Fuc-(1→4)-GlcNAc linkage appeared to be less flexible than the β-GlcNAc-(1→3)-Gal linkage. It remained in the energy well surrounding the **A**′ global minimum identified by the TRIPOS PIM force field throughout the entire simulation with standard deviations of 16° and 24° for Φ^2 and Ψ^2, respectively. The results of the 8 ns simulation at 310 K are shown in Figures 5c, d and 6c, d and support an expected increased flexibility of both glycosidic bonds at this higher temperature. Indeed at 310 K a marked increased flexibility of the β-GlcNAc-(1→3)-Gal linkage was observed. While the average values and standard deviations calculated for Ψ^1 were similar to that obtained at 300 K, the Φ^1 torsion and its associated standard deviation were significantly different from that obtained at 300 K (Table 1, entry 2). Indeed the significantly increased flexibility around that torsion was further seen when looking at the Φ^1–Ψ^1 trajectories for this linkage (Figure 5c) and the variations of the individual Φ^1 torsion (Fig. 6c). While the trisaccharide remained in the low-energy region surrounding the **A** and **B** minima throughout most of the simulation, transitions occurred to the region surrounding the **D** orientation (Fig. 5c) corresponding to Φ^1 orientations between 0° and 60°.

Careful examination of the trajectory followed by the Φ^1 torsion at 310 K (Fig. 6c), showed that once the conformation had reached the local minimum **D** with a Φ^1 value of ~60° (Table 1, entry 5), it remained in that energy well for some time before returning to the energy well surrounding the minima **A** and **B**. In contrast to the drastic conformational change around the GlcNAc-(1→3)-Gal linkage, the α-Fuc-(1→4)-GlcNAc linkage remained in the energy well surrounding the **A**′ minimum throughout the entire simulation (Fig. 5d). The average Φ^2 and Ψ^2 values calculated for the 310 K simulation were similar to that calculated at 300 K and only a small increase in flexibility around Φ^2 was shown by the greater standard deviation obtained for this torsion. While for both the Φ^2 and Ψ^2 torsions significant fluctuations in the torsions adopted were observed such that the entire low-energy region associated with the minimum **A**′ energy well was explored, no transitions were observed to the **B**′ minimum of this linkage. However, this linkage in trisaccharide **2** still shows considerable flexibility when compared to branched trisaccharides containing the same linkage as well as to the corresponding disaccharide.[26]

Overall, the trisaccharide displays significant flexibility in solution. As could be anticipated from the results of the combined rigid and stochastic searches, it readily adopts conformations around the **AA**′ and **BA**′ minima at 300 K but also visits the second local minimum **DA**′ at 310 K. Indeed, 8 ns molecular dynamics simulations at 300 and 310 K starting from this local minimum (**DA**′) confirmed that while visited, the trisaccharide did not maintain extensively the **D** orientation around the β-GlcNAc-(1→3)-Gal linkage (Fig. 7). Indeed, at both temperatures, this glycosidic torsion quickly returned to the minimum energy plateau containing the **A** and **B** orientations, albeit more slowly at 310 K confirming that

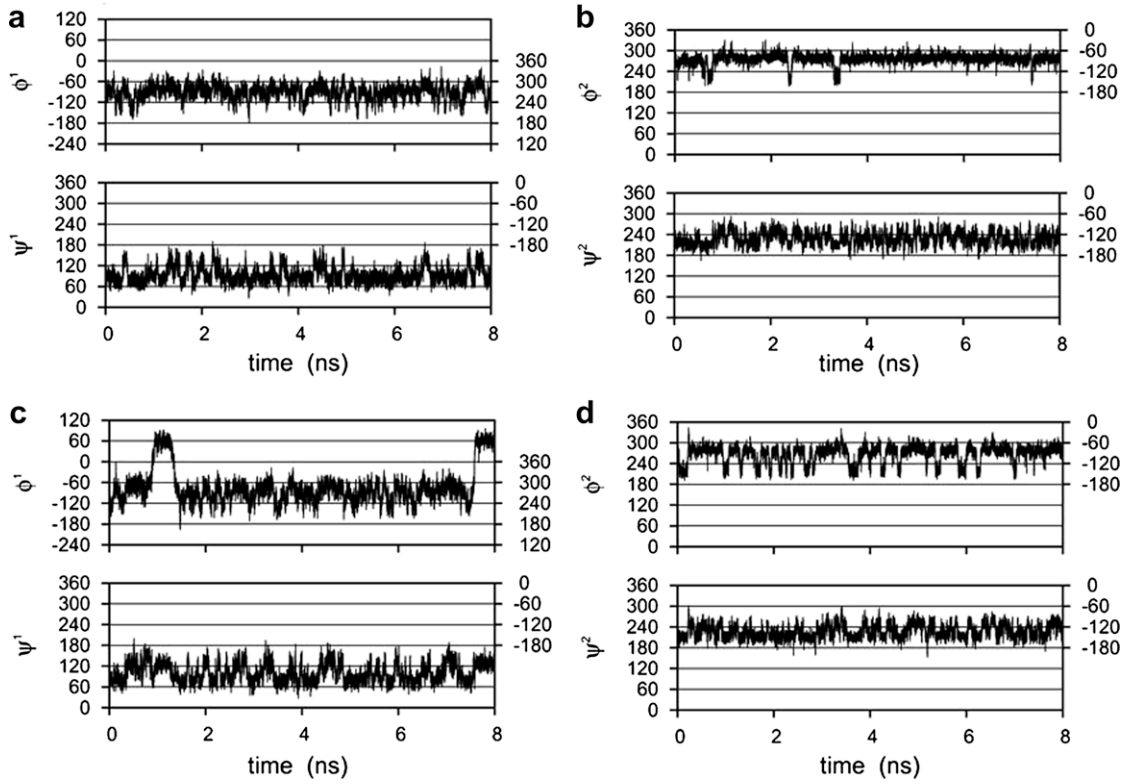

Figure 6. Glycosidic dihedral trajectories during the 8 ns dynamics simulations at 300 K (a and b) and 310 K (c and d). (a) and (c) β-GlcNAc-(1→3)-Gal linkage. (b) and (d) α-Fuc-(1→4)-GlcNAc linkage.

this conformation is more likely to be populated at higher temperatures. As expected, the α-Fuc-(1→4)-GlcNAc linkage in these later simulations remained throughout the simulations in the energy well surrounding the **A**′ minimum (data shown in Supplementary data).

Finally, Figure 8 shows the overlay of 200 conformations extracted from the 8 ns MD simulation at 310 K starting from the global minimum **AA**′. The flexibility of the molecule and the particular flexibility of the β-GlcNAc-(1→3)-Gal linkage are clearly evident.

2.4. Comparison of experimental and theoretical data

Assuming isotropic motion, theoretical $\langle r^{-6} \rangle$ averaged distances were calculated for H-1″/H-4′, H-1′/H-3 and H-1′/H-4 over all of the conformations generated during the MD simulations started from the global minimum **AA**′ at 300 and 310 K (Table 2, entries 1 and 2). Table 2 also gives the distances measured for the global minimum **AA**′ and local minima **BA**′ and **DA**′ selected from the rigid search and minimized with the Tripos-PIM force field (entries 3–5). It is interesting to notice that the H-1′/H-4 distance is substantially longer (>4 Å) for both the **B** and **D** orientations around the GlcNAc-(1→3)-Gal linkage (Table 2, entries 4 and 5) than for the **A** orientation (entry 3). Indeed, the calculated average distance between these two hydrogens is 2.8 Å in both molecular dynamics runs at 300 and 310 K and there is no significant difference in this calculated distance whether the molecule visits the energy plateau surrounding the **D** orientation, or whether it remains in the energy plateau that encompasses the **A** and **B** minima. Therefore, experimental measurement of this distance does not allow confirmation of whether or not the transition to the **DA**′ local minimum effectively occurs at 310 K. Indeed, the distances measured experimentally (ROE) at 300 K are in good agreement (Table 2, entries 1, 2 and 6) with the distances calculated at 300 or 310 K suggesting that the true solution behavior is compatible with both simulation behaviors. The H-1′/H-3 and H-1″/H-4 theoretical and experimental distances agree completely while the H-1′/H-4 distance is larger than that measured for the global minimum **AA**′ and well within experimental range of the calculated distances at 300 and 310 K. Thus while the α-Fuc-(1→4)-GlcNAc linkage adopts predominantly the **A**′ type orientation with very little contribution from the **B**′ orientation the GlcNAc-(1→3)-Gal linkage is likely sampling the **A** and **B** orientation as well as possibly the **D** as observed in the 310 K molecular dynamics simulation (Fig. 4c). Overall, in terms of the conformations of the trisaccharide, these favored orientations of the glycosidic linkages support the presence of significant populations of trisaccharide conformational families **AA**′, **BA**′ and **DA**′ in solution. The extensive flexibility of both glycosidic linkages suggests that the distinct conformational families of the trisaccharide can readily interconvert in solution.

3. Conclusion

We have outlined a more efficient synthesis and the major conformational features of a trisaccharide fragment of the Le^aLe^x hexasaccharide tumor antigen as part of our ongoing efforts to identify internal epitopes that may be useful in the development of anticancer vaccines. Explorations of the conformational space occupied by the trisaccharide were carried out using the unprecedented combination of a rigid systematic search as implemented in Sybyl and using the Tripos force field along with the PIM parameters and a stochastic search as implemented in MOE2004 and using the Amber94 force field. Indeed, we have shown that the two methods complement each other well and, in this case, allow the identification of three conformations that are energetically relevant. Molecular dynamics simulations in explicit water using the Amber9 force field with the inclusion of the Glycam parameters confirmed that this linear trisaccharide was highly flexible. Dynamic simulations starting from the global minimum at 300 K showed that two of

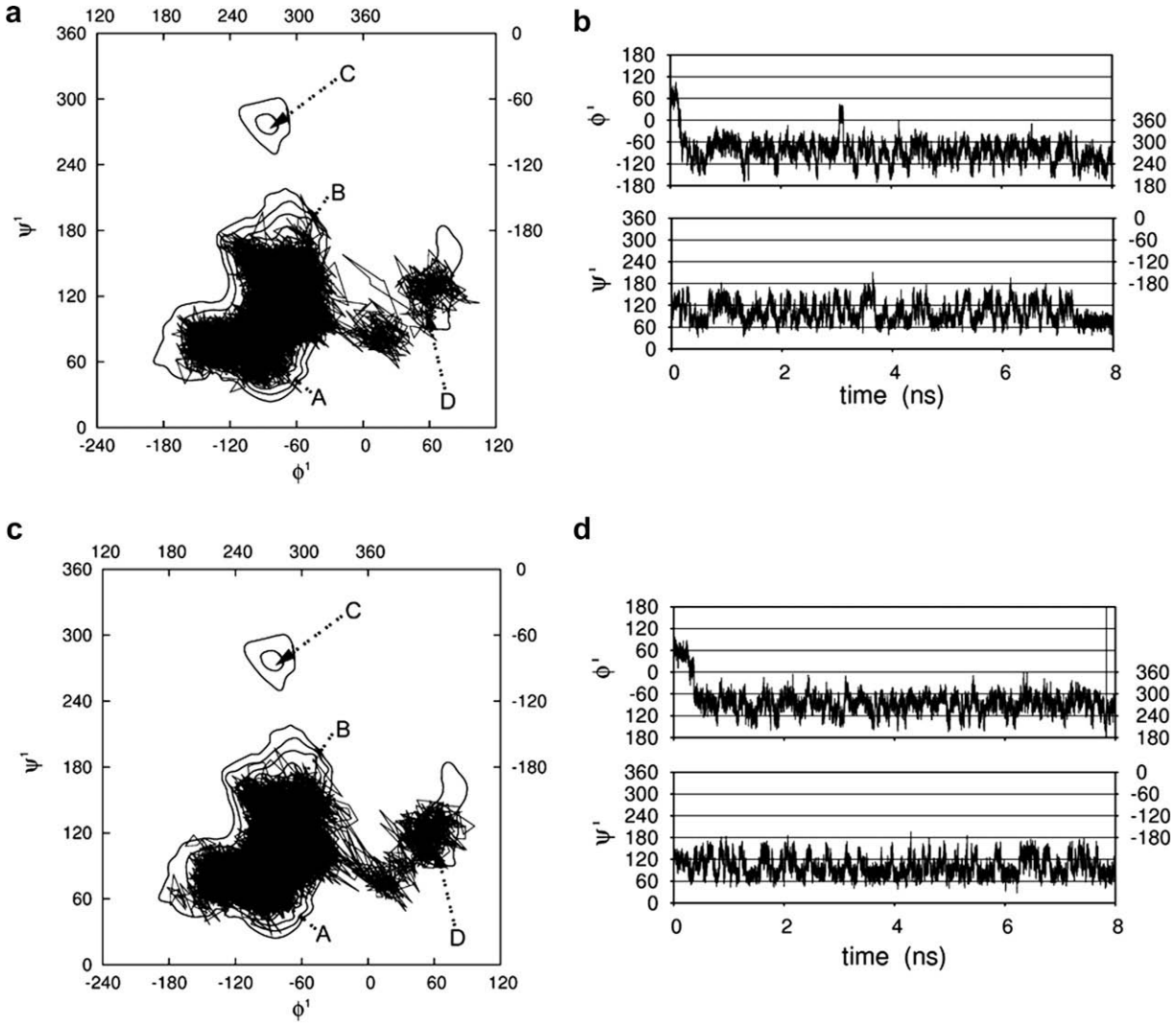

Figure 7. Trajectories of the glycosidic torsion angles Φ^1, Ψ^1 for the β-GlcNAc-(1→3)-Gal linkage during the 8 ns dynamics simulations starting from the local minimum D. Simulations (a) and (b) at 300 K; (c) and (d) at 310 K. For (a) and (c) the trajectories are superimposed on the MM3 grid search energy maps obtained for the disaccharide linkages (contours).[19] The main minima identified in the PIM rigid systematic search are labeled **A**–**D**.

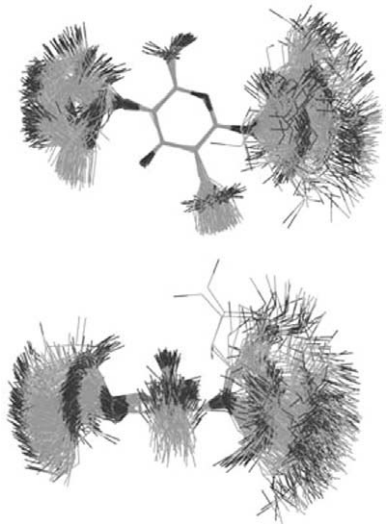

Figure 8. Overlay of 200 snapshots from the 8 ns molecular dynamics simulation at 310 K.

Table 2
Calculated and measured inter-proton distances

Entry		H-1′/H-3 (Å)	H-1′/H-4 (Å)	H-1″/ H-4′ (Å)
Molecular dynamics simulations[a]				
	T (K)			
1	300	2.2	2.8	2.2
		±0.2[b]	±0.8[b]	±0.2[b]
2	310	2.3	2.8	2.2
		±0.5[b]	±1.0[b]	±0.2[b]
Rigid search conformations[c]				
3	**AA**′	2.4	2.6	2.2
4	**BA**′	2.6	4.4	2.2
5	**DA**′	3.6	4.1	2.2
NMR measurements				
6		2.3	3.2	2.4

[a] Average distances calculated for the MD simulations.
[b] Standard deviation.
[c] Selected from the rigid search and minimized with the Tripos-PIM force field.

the three conformers identified by the combined systematic and stochastic searches were visited while simulations at 310 K showed that the third conformation was also accessible. The theo-

retical distances averaged from these dynamic simulations were matched to the NOE derived distances confirming that the trisaccharide was highly flexible in solution. However, because the experimental distances measured from the NOE buildup curves were in good agreement with the distances calculated from both sets of dynamic simulations starting from the global minimum at 300 and 310 K, it was impossible to confirm whether or not both identified local minima were indeed populated in solution. The β-GlcNAc-(1→3)-Gal linkage was shown to be particularly flexible adopting a wide range of orientations around these conformations. Additional studies to shed light on the conformational behavior of this linkage in the Le^aLe^x hexasaccharide are ongoing in our laboratory and will be reported in due time. However, our preliminary results do indicate that this linkage is, indeed, quite flexible even in the larger hexasaccharide. The flexibility around this central linkage suggests that there may be multiple internal epitopes of the hexasaccharide that can be targeted for anti-cancer vaccine development.

4. Experimental

4.1. Synthesis of fragment 2

4.1.1. Materials and methods

^1H (600, 400 or 300 MHz) and ^{13}C NMR (150, 100 or 75.5 MHz) spectra were recorded for compounds solubilized in $CDCl_3$ or D_2O. ^1H chemical shits were referenced to TMS (δ 0.0, $CDCl_3$) or sodium 2,2-dimethyl-2-silapentane-5-sulfonate (external standard DSS, δ 0.0). Chemical shifts and coupling constants were obtained from a first-order analysis of one-dimensional spectra. Data are reported as s = singlet, d = doublet, t = triplet, q = quartet, m = multiplet, b = broad and coupling constant(s) are in Hertz. ^{13}C chemical shifts were referenced to internal $CDCl_3$ (δ 77.0) or external DSS (δ 0.0). Assignments of proton and carbon resonances were based on COSY and ^{13}C–^1H heteronuclear correlated experiments. Mass spectra were obtained under electron spray ionisation (ESI) on a high resolution mass spectrometer. TLC were performed on precoated aluminum plates with Silica Gel 60 F_{254} and detected with UV light and/or charred with a solution of 10% H_2SO_4 in EtOH. Compounds were purified by flash chromatography with Silica Gel 60 (230–400 mesh) unless otherwise stated. Solvents were distilled and dried according to standard procedures,[27] and organic solutions were dried over Na_2SO_4 and concentrated under reduced pressure below 40 °C. Centrifugal chromatography was performed on a silica gel plate (2 mm thickness). Optical rotation measurements were uncorrected.

4.1.2. Methyl 3,4-di-*O*-[3,4,6-tri-*O*-acetyl-2-deoxy-2-(2,2,2-trichlorethoxycarbonylamino)-2,6-di-*O*-benzoyl-β-D-glucopyranosyl]-β-D-galactopyranoside (5)

The donor **3** (22.2 mg, 0.04 mmol), the acceptor **4** (21.2 mg, 0.05 mmol) and activated powdered 4 Å MS (200 mg) were stirred in CH_2Cl_2 (2 mL) at room temperature under N_2 for 1 h. The mixture was cooled to −78 °C, TMSOTf (0.28 M in CH_2Cl_2, 22.3 μL, 6.2 μmol) was added, and the mixture was allowed to warm to room temperature overnight. The mixture was cooled to −78 °C, additional TMSOTf (0.28 M in CH_2Cl_2, 45.0 μL, 13 μmol) was added and the mixture was again allowed to warm to room temperature overnight. Et_3N (5 μL) was added, the mixture was filtered, the solids were washed with CH_2Cl_2 and the filtrate and washings were combined and concentrated. Chromatography (6:4 to 1:1 hexanes–EtOAc) gave trisaccharide **5** (18.0 mg, 76%) pure as an amorphous solid. $[\alpha]_D$ = +6 (*c* 0.7, $CHCl_3$). ^1H NMR (400 MHz, $CDCl_3$): δ 7.38–8.15 (m, 10H, Ar), 6.06 (d, 1H, *J* = 8.8 Hz, NH′), 5.42 (t, 1H, *J* = 9.1 Hz, H-3′), 5.32 (t, 1H, *J* = 10.0 Hz, H-2), 5.23 (d, 4H, *J* = 8.6 Hz, H-1), 5.19–4.95 (m, 4H, H-3″, H-5″, OCH_2CCl_3), 4.91 (d, 1H, *J* = 8.7 Hz, NH″), 4.72 (d, 1H, *J* = 12.2 Hz, OCH*H*CCl_3), 4.68–4.62 (m, 2H, H-6″a, OCH*H*CCl_3), 4.59 (d, 1H, *J* = 8.2 Hz, H-1″), 4.53–4.42 (m, 3H, H-1′, H-4′, H-6″b), 4.40–4.32 (m, 2H, H-5′, H-6a), 4.21 (dd, 1H, *J* = 3.8, 12.2 Hz, H-6′a), 4.10 (br d, 1H, *J* = 10.5 Hz, H-6b), 4.00 (br d, 1H, *J* = 11.3 Hz, H-6′b), 3.96–3.82 (m, 3H, H-3, H-4, H-2″), 3.72–3.63 (m, 2H, H-5, H-4″), 3.59 (t, 1H, *J* = 9.1 Hz, H-2″), 3.44 (s, 3H, CH_3O), 2.18–1.92 (6s, 6 × 3H, 6 × CH_3CO). ^{13}C NMR (100 MHz, $CDCl_3$): δ 170.0 (CO), 133.8, 133.6, 130.0, 129.9, 129.0, 128.8 (Ar), 101.8 (C-1″, 101.2 (C-1′), 99.8 (C-1), 79.9 (C-3 or C-4 or C-2′), 74.7 (OCH_2CCl_3), 72.6, 72.2 (C-3 or C-4 or C-2′, C-2, C-5, C-3′, C-4′, C-5′, C-3″, C-4″, C-5″), 70.7 (OCH_2CCl_3), 69.2 (C-6″), 68.8 (C-6), 62.3 (C-6′), 62.1 (C-2), 56.9 (C-3 or C-4 or C-2′, C-2″), 56.4 (CH_3O), 21.0, 20.8 (*C*H_3CO). HRMS calcd for $C_{51}H_{58}Cl_6N_2O_{26}$ $[M+K]^+$ 1363.1046, found 1363.1057.

4.1.3. Methyl 2,4,6-tri-*O*-benzoyl-β-D-galactopyranoside (6)

Diol **4** (1.2 g, 3.0 mmol) was dissolved in CH_2Cl_2 (42 mL), trimethylorthobenzoate (1.8 mL, 10 mmol) and TsOH (42 mg, 0.25 mmol) were added and the mixture was stirred 1 h under N_2 at room temperature. Et_3N (40 μL) was added to the reaction mixture, and solvents were evaporated. The residue was dissolved in 80% AcOH–H_2O (55 mL), and the solution was stirred at room temperature for 2-h. Solvents were removed by co-evaporation with toluene, and chromatography of the residue (7:3 hexanes–EtOAc) gave acceptor **6** (1.22 g, 81%) pure as a colorless glass. ^1H NMR (400 MHz, $CDCl_3$): δ 7.39–8.17 (m, 15 H, Ar), 5.78 (d, 1H, *J* = 3.4 Hz, H-4), 5.38 (dd, 1H, *J* = 7.9, 10.0 Hz, H-2), 4.63 (d, 1H, *J* = 7.9 Hz, H-1), 4.60 (dd, 1H, *J* = 6.8, 11.3 Hz, H-6a), 4.42 (dd, 1H, *J* = 6.2, 11.4 Hz, H-6b), 4.18–4.05 (m, 2H, H-3, H-5), 3.57 (s, 3 H, CH_3O). ^{13}C NMR (100 MHz, $CDCl_3$): δ 166.8, 166.4, 166.2 (CO), 133.7, 133.5, 133.4, 130.2, 130.0, 129.9, 129.6, 129.2, 128.7, 128.6, 128.5 (Ar), 102.2 (C-1), 73.6 (C-2), 71.9 (C-3 or C-5), 71.5 (C-3 or C-5), 70.6 (C-4), 62.5 (C-6), 57.2 (CH_3O). The NMR data agreed with that previously reported.[12]

4.1.4. Methyl 3-*O*-[3,4,6-tri-*O*-acetyl-2-deoxy-2-(2,2,2-trichlorethoxycarbonylamino)-β-D-glucopyranosyl]-2,4,6-tri-*O*-benzoyl-β-D-galactopyranoside (7)

The acceptor **6** (175 mg, 0.35 mmol), the donor **3** (374 mg, 0.60 mmol) and activated powdered 4 Å molecular sieves (480 mg) were stirred in CH_2Cl_2 (6.4 mL) at room temperature under N_2 for 1 h. The mixture was cooled to −60 °C, TMSOTf (64 μL, 0.35 mmol) was added, and the mixture was stirred at −30 °C overnight. Et_3N (45 μL) was added to the reaction mixture; the solids were filtered off, washed with CH_2Cl_2 and the filtrate and washings were combined and concentrated. Chromatography (8:2 to 1:1 hexanes–EtOAc) of the residue gave disaccharide **7** (296 mg, 88%) pure as colorless glass. $[\alpha]_D$ = +38 (*c* 2.3, $CHCl_3$). ^1H NMR (400 MHz, $CDCl_3$): δ 8.17–7.37 (m, 15H, Ar), 5.85 (d, 1H, *J* = 3.2 Hz, H-4), 5.62 (dd, 1H, *J* = 7.9, 9.9 Hz, H-2), 5.37 (t, 1H, *J* = 9.9 Hz, H-3′), 5.01 (d, 1H, *J* = 8.0 Hz, H-1′), 4.94 (t, 1H, *J* = 9.6 Hz, H-4′), 4.89 (d, 1H, *J* = 7.7 Hz, NH), 4.57 (d, 1H, *J* = 7.9 Hz, H-1), 4.53 (dd, 1H, *J* = 5.3, 11.7 Hz, H-6a), 4.48 (dd, 1H, *J* = 7.1, 11.7 Hz, H-6b), 4.26–4.06 (m, 5H, H-3, H-5, H-6′a, H-6′b, OC*H*$HCCl_3$), 3.79–3. 62 (m, 2H, H-5′, OCH*H*CCl_3), 3.50 (s, 3 H, CH_3O), 3.20 (q, 1 H, *J* = 8.8 Hz, H-2′), 1.97, 1.89 (3s, 3 × 3H, 3 × CH_3CO). ^{13}C NMR (100 MHz, $CDCl_3$): δ 171.1, 166.5, 165.3 (CO), 133.7, 133.5, 130.5, 130.2, 130.0, 129.8, 128.9, 128.8, 128.7 (Ar), 102.4 (C-1, C-1′), 95.6 (CCl_3), 78.1 (C-3 or C-5), 73.8 (OCH_2CCl3), 72.1 (C-3 or C-5), 71.9 (C-2), 71.5 (C-3′), 70.3 (C-4), 68.9 (C-4′), 63.3 (C-6), 61.8 (C-6′), 57.2 (CH_3O), 56.8 (C-2′), 20.9, 20.9, 20.7 (*C*H_3CO). HRMS calcd for $C_{43}H_{44}Cl_3NO_{18}$ $[M+NH_4]^+$ 985.1968, found 985.1971.

4.1.5. Methyl 2,4,6-tri-*O*-benzoyl-3-*O*-[2-deoxy-2-(2,2,2-trichlorethoxycarbonylamino)-β-D-glucopyranosyl]-β-D-galactopyranoside (8)

AcCl (400 μL) was added to a solution of disaccharide **7** (206 mg, 0.21 mmol) in MeOH (5 mL) and the reaction mixture was stirred overnight under N_2 at room temperature. Solid $NaHCO_3$ was added to the reaction mixture, solids were filtered off and washed with MeOH (10 mL). The filtrate and washings were combined, concentrated and chromatography of the crude residue (49:1 $CHCl_3$–MeOH) gave triol **8** (138 mg 77%) pure as a colorless glass. $[\alpha]_D$ = +10 (*c* 0.7, MeOH). ^{1}H NMR (400 MHz, $CDCl_3$): δ 8.18–7.38 (m, 15H, Ar), 5.99 (d, 1H, *J* = 3.2 Hz, H-4), 5.56 (dd, 1H, *J* = 8.1, 9.6 Hz, H-2), 5.31 (d, 1H, *J* = 6.7 Hz, NH), 4.81 (br d, 1H, *J* = 6.4 Hz, H-1′), 4.62–4. 50 (m, 2H, H-1, H-6a), 4.38 (dd, 1H, *J* = 5.8, 11.5 Hz, H-6b), 4.22–4. 01 (m, 3H, H-3, H-5, OC*H*HCCl$_3$), 3.82–3.52 (m, 6H, H-3′, H-6′a, H-6′b, OCH*H*CCl$_3$, 2 × OH), 3.51 (s, 1H, CH_3O), 3.27 (br s, 1H, H-5′), 3.28 (br s, 1H, H-4′), 2.85 (br s, 1H, H-2′), 2.00 (br s, 1H, OH). ^{13}C NMR (100 MHz, $CDCl_3$): δ 167.0, 166.6, 165.7, 154.6 (CO), 134.2, 133.8, 130.7, 130.4, 130.1, 129.9, 129.4, 129.0, 128.9 (Ar), 102.6 (C-1, C-1′), 76.2, 71.7, 70.9 (C-2, C-3, C-4, C-5, C-3′, C-4′, C-5′, OCH_2CCl3), 62.7 (C-6), 61.6 (C-6′), 58.8 (C-2′), 57.4 (CH_3O). HRMS calcd for $C_{37}H_{38}Cl_3NO_{15}$ $[M+Na]^+$ 864.1205, found 864.1160.

4.1.6. Methyl 3-*O*-[3-*O*-acetyl-4,6-*O*-benzylidene-2-deoxy-2-(2,2,2-trichlorethoxycarbonylamino)-β-D-glucopyranosyl]-2,4,6-tri-*O*-benzoyl-β-D-galactopyranoside (10)

Benzaldehyde dimethyl acetal (480 μL, 3.20 mmol) and TsOH (92 mg, 0.53 mmol) were added to a solution of triol **8** (1.28 g, 1.52 mmol) in DMF (29 mL) and the solution was stirred at 80 °C for 1 h. Et_3N (80 μL) was added to the reaction mixture, solvents were evaporated and the crude residue was dissolved in pyridine (10 mL) and Ac_2O (5 mL). The solution was stirred under N_2 at room temperature for 1.5 h diluted with water (~20 mL) and extracted with CH_2Cl_2 (3 × ~20 mL). The combined organic phases were washed successively with 1 M HCl, satd aq $NaHCO_3$ and water and the aqueous layers were re-extracted with CH_2Cl_2. The organic layers were combined, dried, concentrated, and chromatography (3:1 hexanes–EtOAc) of the residue gave disaccharide **10** (1.38 g, 94%) pure as an amorphous powder. $[\alpha]_D$ = +13 (*c* 3.1, $CHCl_3$). ^{1}H NMR (400 MHz, $CDCl_3$): δ 8.18–7.31 (m, 20H, Ar), 5.81 (d, 1H, *J* = 2.9 Hz, H-4), 5.62 (dd, 1H, *J* = 8.1, 9.7 Hz, H-2), 5.42 (s, 1 H, C*H*Ph), 5.25 (t, 1H, *J* = 9.8 Hz, H-3′), 4.82 (d, 1H, *J* = 8.2 Hz, H-1′), 4.73 (d, 1H, *J* = 8.6 Hz, NH), 4.57 (d, 1H, *J* = 7.9 Hz, H-1), 4.54–4. 46 (m, 2H, H-6a, H-6b), 4.31 (dd, 1H, *J* = 4.8, 10.7 Hz, H-6′a), 4.20–4.10 (m, 3H, H-3, H-5, OC*H*HCCl$_3$), 4.03 (d, 1H, *J* = 12.2 Hz, OCH*H*CCl$_3$), 3.67 (t, 1H, *J* = 10.2 Hz, H-6′b), 3.59–3.32 (m, 6H, H-2′, H-4′, H-5′, CH_3O), 1.91 (s, 3H, CH_3CO). ^{13}C NMR (100 MHz, $CDCl_3$): δ 166.6, 165.4 (CO), 137.2, 133.9, 133.7, 130.3, 130.1, 129.5, 129.1, 128.9, 128.6, 126.5 (Ar), 102.6, 101.7 (C-1, C-1′, *C*HPh), 95.8 (CCl_3), 78.8 (C-3, C-4′), 74.2 (OCH_2CCl_3), 72.1, 71.7, 70.4 (C-2, C-4, C-5, C-3′), 68.7 (C-6′), 66.7 (C-5′), 63.3 (C-6), 57.3 (C-2′, CH_3O), 21.0 (*C*H_3CO). HRMS calcd for $C_{46}H_{44}Cl_3NO_{16}$ $[M+H]^+$ 972.1804, found 972.1762.

4.1.7. Methyl 3-*O*-[3-*O*-acetyl-6-*O*-benzyl-2-deoxy-2-(2,2,2-trichlorethoxycarbonylamino)-β-D-glucopyranosyl]-2,4,6-tri-*O*-benzoyl-β-D-galactopyranoside (11)

$NaCNBH_3$ (165 mg, 2.63 mmol) and activated 3 Å molecular sieves (0.66 g) were added to a solution of benzylidene acetal **10** (172 mg, 0.18 mmol) stirred under N_2 at room temperature in anhyd THF (3.8 mL). A solution of HCl in Et_2O (2.0 M, 1.7 mL, 3.4 mmol) was then added dropwise until the evolution of gas had ceased and the mixture remained acidic (litmus paper). The mixture was stirred at room temperature for 45 min, decanted into a separatory funnel and satd aq $NaHCO_3$ (20 mL) was added. The mixture was extracted with CH_2Cl_2 (2 × ~20 mL) and the organic layers were washed with water (30 mL), combined, dried and concentrated. Chromatography (6:4 hexanes–EtOAc) of the residue gave the disaccharide acceptor **11** (148 mg, 86%) pure as a white amorphous powder. $[\alpha]_D$ = +16 (*c* 1.2, $CHCl_3$). ^{1}H NMR (300 MHz, $CDCl_3$): δ 8.15–7.28 (m, 20H, Ar), 5.84 (d, 1H, *J* = 3.0 Hz, H-4), 5.54 (dd, 1H, *J* = 7.9, 9.9 Hz, H-2), 4.98 (t, 1H, *J* = 9.8 Hz, H-3′), 4.81 (d, 1H, *J* = 8.1 Hz, H-1′), 4.74 (d, 1H, *J* = 8.1 Hz, NH), 4.59–4. 45 (m, 5H, H-1, H-6a, H-6b, C*H*$_2$Ph), 4.21 (dd, 1H, *J* = 10.0, 3.1 Hz, H-3), 4.13 (t, 1H, *J* = 7.1 Hz, H-5), 4.03 (dd, 1H, *J* = 11.9 Hz, OC*H*HCCl$_3$), 3.93 (dd, 1H, *J* = 12.1 Hz, OCH*H*CCl$_3$), 3.74 (dd, 1H, *J* = 4.06, 10.4 Hz, H-6′a), 3.79 (dd, 1H, *J* = 10.4 Hz, H-6′b), 3.66 (t, 1H, *J* = *J* = 9.1 Hz, H-4′), 3.50 (br s, 4H, H-5′,CH_3O), 3.29 (q, 1H, *J* = 9.0 Hz, H-2′), 3.07 (br s, 1H, OH), 1.93 (s, 3H, CH_3CO). ^{13}C NMR (75 MHz, $CDCl_3$): δ 172.3, 166.6, 165.7 (CO), 137.5-128.3 (Ar), 108.7 (C-1), 101.7 (C-1′), 95.6 (CCl_3), 77.9 (C-3), 74.6 (C-3′, C-5′), 74.2 (OCH_2CCl_3, *C*H$_2$Ph), 72.0 (C-5), 71.8 (C-2), 70.7 (C-4′), 70.3 (C-4), 69.6 (C-6′), 57.4 (CH_3O, C-2′), 21.0 (*C*H_3CO). HRMS calcd for $C_{46}H_{46}Cl_3NO_{16}$ $[M+Na]^+$ 996.1780, found 996.1779.

4.1.8. Methyl 3-*O*-[3,4-di-*O*-acetyl-6-*O*-benzyl-2-deoxy-2-(2,2,2-trichlorethoxycarbonylamino)-β-D-glucopyranosyl]-2,4,6-tri-*O*-benzoyl-β-D-galactopyranoside (12)

A solution of the alcohol **11** (16.0 mg, 0.02 mmol) in Ac_2O (0.2 mL) and pyridine (0.4 mL) was stirred under N_2 at room temperature for 2 h. Solvents were co-evaporated with toluene, and the crude product was purified by chromatography (6:4 hexanes–EtOAc) to yield the pure diacetate **12** (11.3 mg, 68%). $[\alpha]_D$ = +36 (*c* 0.9, $CHCl_3$). ^{1}H NMR (400 MHz, $CDCl_3$): δ 8.18–7.21 (m, 20H, Ar), 5.88 (d, 1H, *J* = 3.2 Hz, H-4), 5.60 (dd, 1H, *J* = 8.1, 9.7 Hz, H-2), 5.30 (t, 1H, *J* = 9.9 Hz, H-3'), 4.95–4.84 (m, 2H, H-1′, H-4′), 4.77 (d, 1H, *J* = 7.9 Hz, NH), 4.55–4.42 (m, 5H, H-1, H-6a, H-6b, C*H*$_2$Ph), 4.20–4.10 (m, 2H, H-3, OC*H*HCCl$_3$), 4.05 (t, 1H, *J* = 6.3 Hz, H-5), 3.78 (d, 1H, *J* = 12.1 Hz, OCH*H*CCl$_3$), 3.70–3.61 (m, 1H, H-5′), 3.60–3.50 (m, 2H, H-6′a, H-6′b), 3.50 (s, 1H, CH_3O), 3.21 (q, 1H, *J* = 8.9 Hz, H-2′), 1.87 (2s, 2 × 3H, 2 × CH_3CO). ^{13}C NMR (75 MHz, $CDCl_3$): δ 171.8, 166.1, 154.3, 153.2 (CO), 144.1, 138.0, 133.4, 133.3, 133.1, 130.2, 130.0, 130.0, 128.6, 128.4, 127.7 (Ar), 117.1 (CCl_3) 102.2 (C-1, C-1′), 73.6 (OCH_2CCl_3, *C*H$_2$Ph), 73.4, 72.3, 69.9 (C-2, C-4, C-5, C-3′, C-4′), 69.7 (C-6′), 62.9 (C-6), 57.1 (CH_3O), 56.5 (C-2′), 20.6, 20.4 (*C*H_3CO). HRMS calcd for $C_{48}H_{48}Cl_3NO_{17}$ $[M+NH_4]^+$ 1033.2332, found 1033.2343.

4.1.9. Methyl 3-*O*-[3-*O*-acetyl-6-*O*-benzyl-4-*O*-(2,3,4-tri-*O*-benzyl-α-L-fucopyranosyl)-2-deoxy-2-(2,2,2-trichlorethoxycarbonylamino)-β-D-glucopyranosyl]-2,4,6-tri-*O*-benzoyl-β-D-galactopyranoside (15)

Method A. A solution of acceptor **11** (93.1 mg, 0.10 mmol), thioglycoside donor **13** (162 mg, 0.34 mmol) in Et_2O (5 mL) containing activated powdered 4 Å molecular sieves (173 mg) was stirred under N_2 at room temperature for 1 h. MeOTf (53 μL, 0.47 mmol) was added and the mixture was stirred at room temperature for an additional 1.5 h. Et_3N (63 μL) was added to the mixture; the solids were filtered off and washed with Et_2O (~10 mL). The filtrate and washings were combined, concentrated and centrifugal purification (17:3 to 7:3 hexanes–EtOAc) of the crude residue gave trisaccharide **15** (114 mg, 85%) pure as an amorphous powder.

Method B. Coupling of the acceptor **11** (29.6 mg, 0.03 mmol), and thioglycoside **14** (51.5 mg, 0.11 mmol) under MeOTf (20 μL, 0.18 mmol) activation was carried out in Et_2O (1.5 mL) as described above for the coupling of acceptor **11** with donor **13**. Work up, as described above, followed by column chromatography (7:3 hexanes–EtOAc) of the crude residue gave trisaccharide **15** (32.5 mg, 77%) pure.

Analytical data for 15. $[\alpha]_D$ = −3 (*c* 1.8, $CHCl_3$). ^{1}H NMR (300 MHz, $CDCl_3$): δ 8.18–7.15 (m, 35H, Ar), 5.84 (d, 1H, *J* = 2.6 Hz, H-4), 5.58 (br t, 1H, *J* = 8.8 Hz, H-2), 5.02 (br t, 1H,

J = 8.5 Hz, H-3′), 4.90 (d, 1H, J = 11.5 Hz, C*H*Ph), 4.85 (d, 1H, J = 2.4 Hz, H-1″), 4.78–4. 23 (m, 12H, H-1, H-1′, H-6a, H-6b, NH, 7 × C*H*Ph), 4.20–3.88 (m, 5H, H-3, H-5, H-6′a, OCH_2CCl_3), 3.93 (dd, 1H, J = 3.4, 10.2 Hz, H-2″), 3.79–3. 67 (m, 2H, H-3″, H-5″), 3.65–3.41 (m, 7H, H-4′, H-5′, H-6′b, H-4″, CH_3O), 3.24 (q, 1H, J = 8.9 Hz, H-2′), 1.85 (s, 3H, CH_3O), 0.97 (d, 3H, J = 6.4 Hz, H-6″). ^{13}C NMR (75 MHz, $CDCl_3$): δ 170.8, 166.1, 165.0, 153.8 (CO), 138.7, 138.4, 130.2, 130.0, 129.7, 128.6, 128.4, 128.3, 128.2, 128.2, 127.7, 127.7, 127.6, 127.4, 127.3 (Ar), 102.2 (C-1), 101.0 (C-1′), 100.1 (C-1″), 95.4 (CCl_3), 79.0, 77.9, 77.2, 76.5, 75.2, 73.0, 71.8 (C-3, C-5, C-3′, C-4′, C-5′, C-2″, C-4″, C-5″), 74.9 (CH_2), 73.9 (CH_2), 73.8 (CH_2), 73.4 (CH_2), 72.8 (CH_2), 71.5 (C-2), 70.6 (C-4), 69.5 (C-6′), 67.7 (C-3″), 62.9 (C-6), 5.68, 56.6 (CH_3O, C-2′), 21.0 (CH_3CO), 16.3 (C-6″). HRMS calcd for $C_{73}H_{74}Cl_3NO_{20}$ $[M+K]^+$ 1428.3507, found 1428.3438.

4.1.10. Methyl 3-*O*-[3-*O*-acetyl-6-*O*-benzyl-4-*O*-(2,3,4-tri-*O*-benzyl-α-L-fucopyranosyl)-2-deoxy-2-acetamido-β-D-glucopyranosyl]-2,4,6-tri-*O*-benzoyl-β-D-galactopyranoside (16)

Activated Zn dust (65 mg) was added to a solution of trisaccharide **15** (20.6 mg, 0.02 mmol) in Ac_2O (1 mL) and the mixture was stirred under N_2 at room temperature overnight. The solids were filtered off on Celite, washed with AcOH (2 mL) and the combined filtrate and washings were co-concentrated with toluene. Column chromatography (7:1 to 1:1 hexanes–EtOAc) of the residue gave the amide **16** (14.8 mg, 79%) as an amorphous powder. $[\alpha]_D = -6$ (c 0.6, $CHCl_3$). ^{1}H NMR (300 MHz, $CDCl_3$): δ 8.19–7.12 (m, 35H, Ar), 5.84 (d, 1H, J = 3.1 Hz, H-4), 5.57 (dd, 1H, J = 8.1, 9.8 Hz, H-2), 5.04–4.88 (m, 3H, H-3′, NH, C*H*Ph), 4.85 (d, 1H, J = 3.5 Hz, H-1″), 4.80–4.25 (m, 11H, H-1′, H-1, H-6a, H-6b, 7 × C*H*Ph), 4.12 (dd, 1H, J = 9.9, 3.4 Hz, H-3), 4.05–3.93 (m, 2H, H-5, H-6′a), 3.92 (dd, 1H, J = 3.4, 10.2 Hz, H-2″), 3.79–3.68 (m, 2H, H-3″, H-5″), 3.63–3. 37 (m, 8H, H-2′, H-4′, H-5′, H-6′b, H-4″, CH_3O), 1.86 (s, 3H, CH_3COO), 1.28 (s, 3H, CH_3CON), 0.97 (d, 3H, J = 6.4 Hz, H-6″). ^{13}C NMR (75 MHz, $CDCl_3$): δ 173.9, 171.1, 170.0, 166.1, 163.7 (CO) 138.4, 135.2, 133.5, 133.1, 131.4, 130.2, 129.9, 129.7, 129.1, 128.8, 128.7, 128.4, 128.3, 128.2, 128.1, 127.9, 127.7, 127.7, 127.5, 127.4, 127.3, 127.1 (Ar), 102.1 (C-1), 101.5 (C-1′), 99.9 (C-1″), 74.9 (CH_2Ph), 73.8 (CH_2Ph), 73.3 (CH_2Ph), 72.8 (CH_2Ph), 70.0, 71.0, 71.5, 73.8, 73.9, 75.1 (C-3, C-5, C-2′, C-3′, C-4′, C-5′, C-2″, C-3″, C-4″, C-5″), 72.8 (CH_2Ph), 68.5 (C-6′), 67.2 (C-4, C-2), 62.2 (C-6), 56.8 (C-2′, CH_3O), 22.7 (NHCO), 21.1 (CH_3CO), 14.1 (C-6″). HRMS calcd for $C_{72}H_{75}NO_{19}$ $[M+NH_4]^+$ 1275.5277, found 1275.5240.

4.1.11. Methyl 3-*O*-[2-acetamido-6-*O*-benzyl-4-*O*-(2,3,4-tri-*O*-benzyl-α-L-fucopyranosyl)-2-deoxy-β-D-glucopyranosyl]-β-D-galactopyranoside (17)

Trisaccharide **16** (14.7 mg, 0.01 mmol) was dissolved in methanolic sodium methoxide (0.25 M, 1.5 mL), and the mixture was stirred under N_2 at room temperature for 3 h. The mixture was deionized with Dowex 50 (H+) resin, filtered, and solids were washed with MeOH (3 mL). The filtrate and washings were combined and concentrated. Chromatography (19:1 $CHCl_3$–MeOH) of the residue gave trisaccharide **17** (8.3 mg, 79%) pure. $[\alpha]_D = -25$ (c 0.5, $CHCl_3$). ^{1}H NMR (400 MHz, $CDCl_3$): δ 7.43–7. 17 (m, 20H, Ar), 6.72 (br s, 1H, NH), 5.22 (d, 1H, J = 8.4 Hz, H-1′), 4.97 (d, 1H, J = 11.4 Hz, C*H*Ph), 4.92 (d, 1H, J = 3.7 Hz, H-1″), 4.85–4.58 (m, 5H, 5 × C*H*Ph), 4.27 (d, 1, J = 12.0 Hz, C*H*HPh), 4.20 (d, 1 H, J = 11.9 Hz, CH*H*Ph), 4.16 (d, 1H, J = 7.8 Hz, H-1), 4.12–3.96 (m, 3H, H-3′, H-5″, H-2″), 3.93–3.52 (m, 11H, H-2, H-3, H-5, H-6a, H-6b, H-5′, H-6′a, H′6b, H-3″, H-4″, CH_3O,), 3.31 (t, 1H, J = 8.7 Hz, H-4′), 3.17 (q, 1H, J = 8.3 Hz, H-2′), 1.98 (s, 3H, CH_3CON), 1.14 (d, 3H, J = 6.4 Hz, H-6″). ^{13}C NMR (75 MHz, $CDCl_3$): δ 172.1 (CO), 138.5 138.4 138.1 128.5 128.4 128.3 127.9 127.8 127.7 127.5 (Ar), 104.0 (C-1), 100.1 (C-1′), 99.9 (C-1″), 83.0 (C-3), 81.0 (C-4′), 79.0 (C-5), 75.9 (CH_2Ph), 75.0 (C-4″), 74.2 (CH_2Ph), 74.0 (C-4), 73.1 (CH_2Ph), 72.9 (CH_2Ph), 72.2 (C-3″), 70.0 (C-3′), 69.2 (C-6), 68.4 (C-5′), 68.1 (C-2″), 62.5 (C-6′), 58.2 (C-2″), 57.1 (CH_3O), 23.6 (CH_3CON), 16.7 (C-6″). HRMS calcd for $C_{49}H_{61}NO_{15}$ $[M+NH_4]^+$ 926.3939, found 926.3922.

4.1.12. Methyl 3-*O*-[2-acetamido-2-deoxy-4-*O*-(α-L-fucopyranosyl)-β-D-glucopyranosyl]-β-D-galactopyranoside (2)

Trisaccharide **16** (44.2 mg, 0.04 mmol) was dissolved in methanolic sodium methoxide (1 M, 2.5 mL), and the mixture was stirred at room temperature for 1.5 h. Work up of the reaction was carried out as described above and the crude trisaccharide **17** was filtered through a bed of silica gel eluted with a mixture of $CHCl_3$–MeOH (19:1). After concentration, the semi crude trisaccharide **17** was dissolved in MeOH (4 mL), 10% Pd/C (71.2 mg) was added and the mixture was stirred overnight at room temperature under H_2 atmosphere at 200 psi. The solids were filtered off on Celite, washed with MeOH (8 mL) and the combined filtrate and washings were concentrated. Lyophilization of the residue from water gave trisaccharide **2** (17.6 mg, 92%) as a white amorphous powder: $[\alpha]_D = -93$ (c 0.2, H_2O). ^{1}H NMR (600 MHz, D_2O, 300 K): δ 4.95 (d, 1H, J = 3.8 Hz, H-1″), 4.69 (d, 1H, J = 8.4 Hz, H-1′), 4.34 (q, 1H, J = 6.6 Hz, H-5″), 4.29 (d, 1H, J = 8.0 Hz, H-1), 4.13 (d, 1H, J = 3.2 Hz, H-4), 3.94 (dd, 1H, J = 2.0, 12.3 Hz, H-6′a), 3.85 (dd, 1H, J = 4.2, 12.3 Hz, H-6′b), 3.82 (dd, 1H, J = 3.2, 10.5 Hz, H-3″), 3.75–3.66 (m, 7H, H-6a, H-6b, H-2′, H-2″, H-4″), 3.66–3.58 (m, 3H, H-3, H-5, H-3′), 3.56–3.48 (m, 6H, H-2, H-4, H-5′, CH_3O), 2.03 (s, 1H, NHCO), 1.15 (d, 1H, J = 6.7 Hz, H-6″). ^{13}C NMR (150 MHz, $CDCl_3$): δ 175.3 (CO), 104.2 (C-1), 102.9 (C-1′), 99.9 (C-1″), 82.6 (C-3), 77.4 (C-4′), 75.4 (C-5′), 75.1 (C-5), 72.7 (C-3′), 72.3 (C-4″), 70.1 (C-3″), 69.8 (C-2), 68.7 (C-2″), 68.4 (C-4), 67.4 (C-5″), 61.3 (C-6, C-6″), 57.6 (CH_3O), 56.6 (C-2′), 22.5 (CH_3CO), 15.6 (C-6″). HRMS calcd for $C_{49}H_{61}NO_{15}$ $[M+Na]^+$ 926.3939, found: 926.3922. The NMR data agreed with that previously reported.[8]

4.2. Nuclear magnetic resonance spectroscopy

4.2.1. Sample preparation

Trisaccharide **2** (12.4 mg) was lyophilized three times from D_2O (95%) and then dissolved in 0.7 mL of D_2O (99.96%) to give a final 0.033 M concentration.

4.2.2. NMR experiments

NMR experiments were recorded in 5 mm NMR tubes at 400 MHz (HSQC) and 600 MHz (^{1}H, ^{13}C, COSY, HMBC, NOESY and ROESY). All spectra were recorded at 300 K with the exception of NOESY experiments, which were also recorded at 310 K.

Phase-sensitive two-dimensional NOESY spectra were acquired with a spectral width of 5000 Hz, 2048 complex data points and 64 scans each for 128 increments. A 1.5 s relaxation delay was implemented between scans. NOESY spectra were recorded at seven mixing times: 100 ms increments from 400 ms to 1 s. Before Fourier transformation a $\pi/2$ shifted sine squared window was applied in both dimensions and the FID was zero-filled to 2048 points in the F2 direction and 512 points in the F1 direction. Further handling of the NOESY spectra and integrations of the cross-peaks to obtain buildup curves is described in Supplementary data.

One-dimensional ROESY spectra were acquired with selective excitations of anomeric protons effected using a 60 ms Gaussian-shaped pulse and a spin-lock field of 2.0 kHz. A 5 s relaxation delay was implemented between scans. ROESY spectra were recorded at eleven mixing times from 20 ms to 400 ms. Before Fourier transformation, the FIDs were zero-filled once and multiplied with a 1 Hz line broadening factor. Spectra were phase and baseline corrected and integrated. The integrals measured for the irradiated H-1′ and H-1″ signals were plotted against mixing time and the obtained curves were fitted to a double exponential decaying function:

$$f(\tau_m) = -A[\exp(B\tau_m) - \exp(C\tau_m)]$$

where τ_m is the mixing time and A, B and C are adjustable parameters. The values of these integrals were extrapolated to 0 ms mixing time, and the integrals from cross-relaxation peaks were normalized through division by these extrapolated values. The normalized cross-relaxation integrals were plotted against the mixing times and the buildup curves were fitted to a double exponential equation of the form

$$f(\tau_m) = A[\exp(B\tau_m) - \exp(C\tau_m)]$$

and the initial slopes at 0 ms mixing times were determined from the calculated first derivatives, $f'(0) = A(B - C)$.[28]

Interproton distances were calculated based on the isolated spin pair approximation (ISPA):

$$r_{ij} = r_{ref}(S_{ref}/S_{ij})^{1/6}$$

where S is the initial slope at $\tau_m = 0$, and r is the proton-proton distance. The H-1′/H-3′ intra-residue cross-peak was used as the reference for the distance determinations. The reference distance used was 2.62 Å.

4.3. Computational methods

4.3.1. Sybyl systematic search

A rigid search was carried out in Sybyl7.1[17] using the Tripos force field along with PIM parameters[18] developed for carbohydrates. The starting molecule was built in Sybyl. To eliminate excessive biasing energies from steric interactions associated with rigid positions of ring substituents normally expected to be highly flexible, hydroxyl hydrogen atoms were removed and the hydroxymethyl groups were converted to methyl groups. During the search, the individual monosaccharide rings were held fixed, and the glycosidic Φ and Ψ torsions were varied in 10° increments throughout the entire possible conformational space, and energies were evaluated after each variation. The van der Waals radius scale factors were reduced to very low values (0.3). Electrostatic contributions were not taken into account. Conformations within 40 kcal mol^{-1} of the global minimum were saved and the minima within 3 kcal mol^{-1} of the global minimum were identified. The glycosidic torsions obtained for these minima were then applied to the starting molecule containing all hydrogen atoms and hydroxymethyl groups, and for each minimum, structures containing the nine different combinations of staggard orientations of the hydroxymethyl groups were generated. Each structure was optimized using conjugate gradient minimization with a 0.05 kcal mol^{-1} gradient termination criteria and a 10,00,000 iteration limit. A cutoff of 8 Å was used for nonbonding interactions. For the optimization, electrostatic contributions were taken into account, and a dielectric constant of 78.5 was employed. The lowest energy structure found for each minimum was used as the representative molecule for distance determinations (Table 1).

4.3.2. MOE stochastic search

The trisaccharide was subjected to all atom and heavy atom stochastic conformational searches using the AMBER94 force field[21] in the Molecular Operating Environment (MOE2004)[22] program suite. In this implementation of AMBER94, any parameters missing for a class of compound are approximated by MOE based on parameter values for similar molecular fragments. The starting structure was built using the carbohydrate builder in MOE2004 and submitted to the stochastic search. This search is similar to the random incremental pulse search (RIPS) method[29] in which the coordinates of each atom are randomly perturbed, after which the entire molecule is minimized to attempt to generate a new conformer. In these stochastic searches, new conformations are generated by the rotation of all bonds (including ring bonds) to random dihedral angles. In our searches a bias of 30° was used. This means that dihedral angles were selected with a sum-of-Gaussians distribution with peaks at multiples of 30°. In addition to bond rotations, atom positions were randomly perturbed by 0.4 Å. These random perturbations were repeated 150,000 times per conformational search and each generated conformer was subjected to 500 steps of minimization with full degrees of freedom with implicit solvation by the Generalized Born/Surface Area (GB/SA) continuum solvation model[23] using a dielectric constant of 78. Two separate searches were performed and the databases were combined for analysis. Initially each new conformation was checked against the previously found conformations using a root-mean-square (RMS) tolerance of 0.1 Å on all atoms, including the hydrogen atoms to account for possible hydrogen bonding. The second search was carried out using a more stringent RMS value (0.01 Å) applied to the heavy atoms only. In both searches the calculations terminated at the end of the 150,000 iterations as the number of failures criteria to find new conformations (10,000 iterations in a row) was never met. Structures that did not have the $^4C_1$ conformation for D-glucosamine or D-galactose or those that did not maintain a $^1C_4$ conformation for L-fucose were eliminated. The results of the two searches were combined for analysis. And conformations with energies over 10 kcal/mol above the global minima were rejected resulting in 1450 structures.

4.3.3. Molecular dynamics simulations

The molecular dynamics simulations were carried out using the SANDER module of AMBER9[24] with the inclusion of Glycam04 parameters[25] for carbohydrates. The initial structure was built using the XLEAP module of AMBER. The molecule was solvated with 10 shells of TIPS3P water molecules[30] giving a total of 1070 solvent molecules in a 30 Å cubic box. Dynamics trajectories of 8 ns were calculated. Each simulation was carried out in five stages using the SANDER module of AMBER. First the water molecules were minimized at constant volume (NVT) whereas the trisaccharide was held fixed. A 1000 cycle limit was employed with 50 cycles of steepest descent followed by conjugate gradient minimization. A 1×10^{-3} kcal mol^{-1} Å gradient convergence criteria was used. A 10 Å cutoff was set, and non-bonded updates were made every 10 steps. The dielectric constant was set to 1. Then, the entire system was minimized without any restraints. A 2500 cycle limit was used with 500 cycles of steepest descent followed by conjugate gradient minimization. Afterward, the system was heated for 20 ps from 0 to 300 K or 310 K with the saccharide weakly restrained. Time steps of 2 fs were used and translational momentum was removed every 1000 steps. Bonds involving hydrogens were constrained using the SHAKE algorithm with 0.00001 Å tolerance. Coordinates were output every 250 steps. The system was then equilibrated at a constant pressure (NPT) of 1 atm for 100 ps with no restraints. Finally, production runs of 8 ns were carried out at 300 or 310 K. The PTRAJ module of AMBER was used to analyze the results.

Acknowledgments

The authors thank the National Sciences and Engineering Research Council of Canada, the University of Guelph, the Canada Foundation for Innovation and the Ontario Innovation Trust for financial support. This work was also made possible by the facilities of the Shared Hierarchical Academic Research Computing Network (SHARCNET: www.sharcnet.ca).

Supplementary data

Supplementary data associated with this article can be found, in the online version, at doi:10.1016/j.bmc.2009.01.020.

References and notes

1. Pettijohn, D. E.; Pfenninger, O.; Brown, J.; Duke, R.; Olsson, L. *Proc. Natl. Acad. Sci. U.S.A.* **1988**, *85*, 802.
2. Stranahan, P. L.; Howard, R. B.; Pfenninger, O.; Cowen, M. E.; Johnston, M. R.; Pettijohn, D. E. *Cancer Res.* **1992**, *52*, 2923.
3. Stranahan, P. L.; LaRoe, J.; McCombs, R.; Goldsmith, A.; Rahim, I.; Overland, M.; Pettijohn, D. E. *Glycoconjugate J.* **1996**, *13*, 741.
4. Lemieux, R. U.; Baker, D. R.; Weinstein, W. M.; Switzer, C. M. *Biochemistry* **1981**, *20*, 199.
5. Pettijohn, D. E.; Stranahan, P. L.; Due, C.; Rønne, E.; Sørenson, H. R.; Olsson, L. *Cancer Res.* **1987**, *47*, 1161.
6. Martensson, S.; Due, C.; Pahlsson, P.; Nilsson, B.; Eriksson, H.; Zopf, D.; Olsson, L.; Lundblad, A. *Cancer Res.* **1988**, *48*, 2125.
7. Battifora, H.; Sørenson, H. R.; Mehta, P.; Ahn, C.; Niland, J.; Hage, E.; Pettijohn, D. E.; Olsson, L. *Cancer* **1992**, *70*, 1867.
8. Jain, R. K.; Kohata, K.; Abbas, S. A.; Matta, K. L. *Carbohydr. Res.* **1988**, *172*, 27.
9. Ogawa, T.; Nukada, T.; Matsui, M. *Carbohydr. Res.* **1982**, *101*, 263.
10. Dullenkopf, W.; Castro-Palomino, J. C.; Manzoni, L.; Schmidt, R. R. *Carbohydr. Res.* **1996**, *296*, 135.
11. Sato, S.; Ito, Y.; Nukada, T.; Nakahara, Y.; Ogawa, T. *Carbohydr. Res.* **1987**, *167*, 197; Windmüller, R.; Schmidt, R. R. *Tetrahedron Lett.* **1994**, *43*, 7927; Cao, S.; Gan, Z.; Roy, R. *Carbohydr. Res.* **1999**, *318*, 75.
12. Kovac, P.; Glaudemans, C. P. J.; Taylor, R. B. *Carbohydr. Res.* **1985**, *142*, 158.
13. Lonn, H. *Carbohydr. Res.* **1985**, *139*, 105; Murphy, P. V.; Hubbard, R. E.; Manallack, D. T.; Wills, R. E.; Montana, J. G.; Taylor, R. J. K. *Bioorg. Med. Chem.* **1998**, *6*, 2421.
14. Imberty, A.; Pérez, S. *Chem. Rev.* **2000**, *100*, 4567.
15. Bundle, D. R. Recognition of Carbohydrate Antigens by Antibody Binding sites. In *Bioorganic Chemistry: Carbohydrates;*; Hecht, S. M., Ed.; Oxford University Press: New York, 1999; pp 370–440.
16. IUPAC-I.U.B. Commission of Biochemical Nomenclature. *Eur. J. Biochem.* **1997**, *243*, 9–9.
17. SYBYL 7.1, Tripos Associates, 1699 S. Hanley Road, Suite 303, St Louis, MO 63144, USA.
18. Imberty, A.; Hardman, K. D.; Carver, J. P.; Pérez, S. *Glycobiology* **1991**, *1*, 631.
19. Imberty, A.; Mikros, E.; Koca, J.; Mollicone, R.; Oriol, R.; Pérez, S. *Glycoconjugate J.* **1995**, *12*, 331; Imberty, A.; Mazeau, K.; Pérez, S.; Rivet, A.; Sabin, C. Disaccharide Database. http://www.cermav.cnrs.fr/cgi-bin/di/di.cgi (accessed August 19, 2008).
20. Lemieux, R. U.; Koto, S.; Voisin, D.. In *ACS Symposium Series*; American Chemical Society: Washington, DC, 1979; Vol. 87, pp 17–29.
21. Cornell, W. D.; Cieplak, P.; Bayly, C. I.; Gould, I. R.; Merz, K. M.; Ferguson, D. M.; Spellmeyer, D. C.; Fox, T.; Caldwell, J. W.; Kollman, P. A. *J. Am. Chem. Soc.* **1995**, *117*, 5179.
22. Chemical Computing Group, Montreal, QC, Canada.
23. Still, W. C.; Tempczyk, A.; Hawley, R. C.; Hendrickson, T. *J. Am. Chem. Soc.* **1990**, *112*, 6127; Qiu, D.; Shenkin, P. S.; Hollinger, F. P.; Still, W. C. *J. Phys. Chem. A* **1997**, *101*, 3005; Schaefer, M.; Karplus, M. A. *J. Phys. Chem.* **1996**, *100*, 1578.
24. Case, D. A.; Darden, T. A.; Cheatham et al., T. E. I. AMBER 9, University of California, San Francisco, 2006.
25. Woods, R. J. *Phys. Chem.* **1995**, *99*, 3832.
26. Mukhopadhyay, C.; Bush, C. A. *Biopolymers* **1991**, *31*, 1731.
27. Armarego, W. L. F.; Perrin, D. D. *Purification of Laboratory Chemicals*, 4th ed.; Elsevier Science Ltd, 1996.
28. Maaheimo, H.; Kosma, P.; Brade, L.; Brade, H.; Peters, T. *Biochemistry* **2000**, *39*, 12778.
29. Chang, G.; Guida, W. C.; Still, W. C. *J. Am. Chem. Soc.* **1989**, *111*, 4379.
30. Jorgensen, W. L.; Chandrasekhar, J.; Madura, J.; Klein, M. L. *J. Chem. Phys.* **1983**, *79*, 926.